Simultaneous Reconstruction and Segmentation with the Mumford-Shah functional for Electron Tomography

Li Shen, Eric Todd Quinto, Shiqiang Wang, Ming Jiang

***Abstract*— Electron micrography (EM) is an important method for determining the three-dimensional (3D) structure of macromolecular complexes and biological specimens. But there are several limitations such as poor signal-to-noise, limitation on range of tilt angles and sub-region subject to electron exposure, unintentional movements of the specimen, with EM systems that make the reconstruction procedure a severely ill-posed problem. A different choice of reconstruction method may lead to different results and create different additional artifacts in reconstructed images. In this paper, we combined the artifacts reduction strategy and the iterative reconstruction algorithm using a Mumford-Shah model. With the combined method, one can not only regularize the ill-posedness and provide segmentation simultaneously but also smooth additional artifacts due to the limited data. We applied the method to both simulated data from the Shepp-Logan phantom and cryo-specimen tomography. The results demonstrate the performance of the method in reducing the noise and artifacts while preserving and enhancing the edges in the reconstructed image.**

I. Introduction

Cryo-electron microscopy is a promising technique for resolving the high-resolution structure of macromolecular complexes. A Transmission Electron Microscope (TEM) focuses electrons in a thin beam that illuminates a small part of the specimen. After the electron-specimen interaction, the projections of the specimen are converted to a grey-scale image (micrograph) by the detector [1]. The specimen is then tilted in the beam and projections from different directions are recorded and can be used to reconstruct the three-dimensional structure of the specimen [2]. The reconstruction problem in electron tomography (ET) is an example of a tomographic inverse problem.

A number of difficulties arise when dealing with the inverse problem in ET that do not appear in X-ray tomography. The specimen may be damaged by the electron-specimen interaction, so the total dose used in the TEM must be limited. When low-dose TEM is used, the micrographs will have poor signal-to-noise (SNR) ratio with significant influence of shot noise. The electron beam illuminates only a small sub-region of the specimen and the specimen can be rotated only through a limited range of tilt angles. These limitations on the range of the tilt angle and sub-region lead to severe ill-posedness. Inversion algorithms using limited data can create artifacts, blurring, or other distortions in their reconstructions [3].

Many reconstruction techniques have been introduced to ET. Among them, Weighted Back-projection (WBP) is most widely used for its speed and simplicity of implementation [4]. In [5] and [6], conical tomography is used to study the structure of integral proteins and WBP is adopted in reconstructing small volumes of the specimen. In [7], conical tilt series of mice retinas were reconstructed using WBP method, refined by projection matching and analyzed using semiautomatic density segmentation. But the WBP method is sensitive to artifacts caused by the limited data problem and poor SNR of projection data. Electron lambda-tomography in [8] reserve the speed and simplicity of WBP but is less sensitive to the artifacts. Because of ill-posedness, regularization methods are needed for the ill-posed problem, especially in cases of limited data. Penalized least square approaches, such as Tikhonov and other regularization methods, were previously utilized in X-ray tomography. Recently the simultaneous reconstruction and evaluation of images has been studied using a Mumford-Shah functional. The regularization terms in the Mumford-Shah functional not only force the smoothness of the images within individual regions but also simultaneously prevent smoothing across image edges. In [3],for limited data, the Mumford-Shah-like level-set approach is exploited to find a segmentation, and by that the singularity set of a function of two-dimensional simulated ET data from a torso phantom.

Our main goal in this article is to generalize the iterative algorithm with a Mumford-Shah model in [9] to the inverse problem in ET. To reduce the artifacts in ET, we combine the artifact reduction strategy in [10] to the reconstruction method. The paper is organized as follows. Sec. II provides the math model of ET and the strategy to reduce the artifacts caused by limited data. Sec. III introduces the proposed algorithm of simultaneous image reconstruction and segmentation and describes our design methodology. Sec. IV presents the experimental results.

II. Tomography

In this section, we provide a brief introduction to the ill-posed problems and the mathematical models of ET. Then we introduce the artifacts reduction strategy.

Let X and Y be Hilbert spaces and $A : X \to Y$ a bounded linear operator. Computing for a given function $f \in X$ the result $Af = g$ is called the *forward problem*. In many applications such as X-ray tomography and electron tomography, the opposite is desired, i.e., to obtain the cause

Li Shen and Ming Jiang are from LMAM, School of Mathematical Sciences, Peking University, Beijing 100871, China (email: shenli@pku.edu.cn)

Eric Todd Quinto is from Department of Mathematics, Tufts University, Medford, MA, U.S.A.

Shiqiang Wang is from College of Life Sciences, Peking University, Beijing 100871, China

978-1-4577-0220-4/16/$31.00 ©2016 IEEE

f for a measurement $g \in Y$ under the operator A. If the operator A is linear and bounded, this is called a *linear inverse problem*. The operator A in the mathematical model for X-ray tomography is the *Radon transform*

$$\mathcal{R}f(\theta, s) = \int_{\mathbb{R}} f\left(s\theta + t\theta^{\perp}\right) dt, \tag{1}$$

where $s \in \mathbb{R}, \theta \in S^1$, and $\theta^{\perp}$ is the unit vector $\pi/2$ radians counterclockwise from θ.

A. Mathematical Model of the Image Formation in TEM

In scattering theory, the scattering potential that fully characterizes the scattering properties of the specimen is given as

$$F(x) := -\frac{2m}{\hbar^2}(V(x) + i\Lambda(x)), \tag{2}$$

where $V : \mathbb{R}^3 \to \mathbb{R}$ is the electrostatic potential and $\Lambda : \mathbb{R}^3 \to \mathbb{R}$ the inelastic potential. The real part of F (F^{re}) has a straightforward physical interpretation in terms of the molecular structure of the specimen whereas the imaginary part F^{im} accounts for the decrease in the flux, due to inelastic scattering, of the non-scattered and elastically scattered electrons. The purpose of ET is to reconstruct the three-dimensional distribution of F^{im} in the specimen.

Assume the imaging system is perfect, then the incident electron wave is a monochromatic plane wave (coherent illumination). After interacting with the specimen, the electron passes through the optics of the electron microscope, The model for the optics is based on the wave nature of imaging electrons, and one can use the scalar theory of diffraction in light optics to describe the diffraction of electron waves. As the electron wave reaches the image plane, the intensity illuminated by a single electron is measured at the detector.

B. Limited data tomography

The damage induced by the electron-specimen interaction limits the application of ET in life sciences and results in the *limited data problem*.When a specimen is irradiated by an electron beam, it gets progressively damaged due to ionization. So the number of electrons used to irradiate the specimen needs to be low enough to preserve the structural integrity of the specimen. As the specimen tilts, the distance that the electrons need to pass through in the specimen increases, and the number of electrons that reach the detector decreases. Hence the images recorded at high tilt angles have poor intensity contrast and can not provide useful information for the reconstruction. Consider the highly simplified setting where the inverse problem in ET is recast as the problem of inverting the x-ray transform when it is sampled on a line complex. Even in this case, limitations on the range of the tilt angle lead to severe ill-posedness. Also for a given positioning of the specimen, only a sub-region is subject to electron exposure. This leads to a *local* tomography problem. As a consequence, the scattering potential is not uniquely determined regardless of the quality of the data at our disposal unless prior information of the sample can be used.

C. Reduction of artifacts in limited angle tomography

In the mathematical model, the limitation on the range of the tilt angle means the data $\mathcal{R}f(\theta, s)$ is known only for $\theta \in S^1_{\Phi} \subsetneq S^1$ and $s \in \mathbb{R}$, where

$$S^1_{\Phi} := \{\theta \in S^1 : \theta = \pm(\cos\phi, \sin\phi), |\phi| < \Phi\}, \tag{3}$$

and the *angular range parameter* Φ is assumed to satisfy $0 < \Phi < \pi/2$. In order to compute a limited angle reconstruction, we therefore have to deal with the *limited angle Radon transform*

$$\mathcal{R}_{\Phi} : f \rightarrowtail \mathcal{R}f|_{S^1_{\Phi} \times \mathbb{R}}, \tag{4}$$

rather than data for all $\theta \in S^1$. The back-projection (or dual operator) for the limited angle Radon transform is given by

$$\mathcal{R}^*_{\Phi} g(x) = \int_{\theta \in S^1_{\Phi}} g(\theta, x \cdot \theta) d\theta. \tag{5}$$

It is well-known in X-ray CT that streak artifacts are present at the end of the limited angular range. We briefly introduce the strategy we use to reduce the artifacts caused by limited angle, and readers can see [10] for details. Although this artifact reduction strategy was originally designed for the filtered back-projection (FBP) algorithm and Lambda tomography, it can also be applied in iterative reconstruction algorithms as well. The method of this artifact reduction strategy is to apply more general weights on the projection data before reconstruction. Define the multiplication operator $\mathcal{K}_{\sigma} : \mathcal{S}(S^1 \times \mathbb{R}) \to \mathcal{S}'(S^1 \times \mathbb{R})$,

$$\mathcal{K}_{\sigma} g(\theta, s) = \kappa_{\sigma}(\theta) g(\theta, s), \tag{6}$$

where $\kappa_{\sigma} : S^1 \to \mathbb{R}$ is a smooth (i.e. C^{∞}) cutoff function.

$$\kappa_{\sigma}(\theta) = exp\left\{\frac{(|\theta| - \Phi + \varepsilon)^2}{(|\theta| - \Phi + \varepsilon)^2 - \sigma^2}\right\} 1_{|\theta| \leq \Phi - \sigma} + 1_{|\theta| > \Phi - \sigma}$$

We combine this artifacts reduction strategy to a simultaneous reconstruction and segmentation method with the Mumford-Shah model which we will explain in the next section.

III. Algorithm Description and Design Methodology

In this section we will introduce the Mumford-Shah approach and a alternative minimization algorithm for the inverse problem in ET.

A. The Mumford-Shah approach

Let $g = \mathcal{R}f^{\dagger}$ be the measured projection data of the object under study with true mass density $f^{\dagger}$. The goal of solving the inverse problem is to find an image f such that $\mathcal{R}f = g$. In ET, $f^{\dagger}$ is referred as the imaginary part F^{im} of scattering potential F in (2).

A simultaneous reconstruction and segmentation can be formulated as finding an image f and a meaningful decomposition $\Omega = R_1 \cup R_2 \cup ... \cup R_l \cup K$ of the image domain Ω, where $R_i \subset \Omega$ are disjoint connected open subsets, K is the union of the boundaries of R_i in Ω. The image f is

an approximation to the true image $f^\dagger$ such that f varies slowly within each R_i and varies rapidly across K between different R_i. To obtain (f, K) we minimize the following Mumford-Shah type functional [11]

$$MS(f,K) := \int_Z |\mathcal{R}f - g|^2 dx + \alpha \int_{\Omega\setminus K} |\nabla f|^2 dx + \beta \text{ length}(K), \tag{7}$$

where Ω is the image domain, Z is the set of all lines passing through Ω, f is a piecewise smooth image, $K \subset \Omega$ are the edges, and $\alpha, \beta \geq 0$. Here $\nabla f = (\frac{\partial f}{\partial x}, \frac{\partial f}{\partial y}, \frac{\partial f}{\partial z})$ is the gradient of f. The objective functional $MS(f, K)$ has three terms: a least squares term, forcing f to match the measured data g; a L^2-penalty term for the gradient of f, forcing f to be smooth everywhere in Ω except at the edges K; and a penalty of K's length, forcing the edges K to be "short".

In applying the Mumford-Shah regularization to practical applications, several issues arise. The primary difficulty comes from the edge set K because it is not easy to represent in computer code and to trace its updates. We follow the approach in [12], where the edges are approximated by smooth edge indicator functions. In order to apply the Mumford-Shah regularization to the ET, we modify the Mumford-Shah penalty with Γ- approximation [12] and combine it with the artifact reduction strategy in section II-C. We minimize the functional

$$AT_{\varepsilon,\sigma}(f,v) = \int_Z |\mathcal{R}_\Phi(f) - \mathcal{K}_\sigma g|^2 dx + \alpha \int_\Omega v^2 |\nabla f|^2 dx + \beta \int_\Omega \left(\varepsilon |\nabla v|^2 + \frac{(1-v)^2}{4\varepsilon}\right) dx, \tag{8}$$

for a small constant $\varepsilon > 0$. Here, $\mathcal{R}_\Phi$ is the limited angle transform defined in (4), the cutoff operator $\mathcal{K}_\sigma$ defined in (6) is applied to projection data g. f is the image and v is an image with the same size as f and $0 \leq v \leq 1$. v is used to indicate the edge set K. The heuristic idea is that if $v \approx 0$ the gradient if f is only penalized a little but the last term is big. If $v \approx 1$ the last term nearly vanishes but the gradient of f is fully taken into account. Therefore $v \approx 0$ represent the presence and $v \approx 1$ the absence of an edge.

For $\varepsilon \to 0$ a minimizer $AT_{\varepsilon,\sigma}$ is an approximated minimizer of $MS(f, K)$, which is a solution to the simultaneous reconstruction and segmentation problem. A minimizer of this modified Mumford-Shah functional should be a solution in which the streak artifacts caused by the limited angle problem are suppressed.

B. Iteration algorithm

To compute a minimizer of $AT_{\varepsilon,\sigma}(f, v)$ we use an alternating minimization scheme described in Algorithm 1. In the first subroutine we keep the edge variable v fixed and minimize $AT_{\varepsilon,\sigma}(f, v)$ in f, then in the second subroutine we keep f fixed and minimize $AT_{\varepsilon,\sigma}(f, v)$ in v. Then repeat this procedure for a number of iterations.

Initial values can be chosen as the zero image and no edges inside the image, i.e. the edge set is set to 1. In our cases, we chose the reconstructed image from *weighted back-projection* (WBP) method as initial image. Thus the iteration time decreases in our experiments. Although $AT_{\varepsilon,\sigma}(f, v)$ is not jointly convex in (f, v), the functional is convex in each variable separately. Therefore, in each of the above mentioned subroutines, we can use iterative gradient descent methods of the form $\phi^{i+1} = \phi^i + c_i d^i$, where ϕ is either f or v, depending on which variable we are considering in the subroutine, d is an appropriate descent direction and c is the step size. The descent direction is derived from the variations $\nabla_f AT_{\varepsilon,\sigma}$ or $\nabla_v AT_{\varepsilon,\sigma}$ respectively.

To compute a descent direction we will also need the adjoint operator of the limited angle Radon transform $\mathcal{R}^*_\Phi$ defined in (5), which is called back projection. The variations of $AT_{\varepsilon,\sigma}$ with respect to (f, v) are

$$\nabla_f AT_{\varepsilon,\sigma}(f,v) = 2\mathcal{R}^*_\Phi(\mathcal{R}_\Phi(f) - \mathcal{K}_\sigma g) - 2\alpha \text{ div}\left(v^2 \nabla f\right),$$

$$\nabla_v AT_{\varepsilon,\sigma}(f,v) = 2\alpha |\nabla f|^2 v + \frac{\beta}{2\varepsilon}(v-1) - 2\beta\varepsilon\Delta v,$$

where $\Delta v = \frac{\partial v}{\partial x}^2 + \frac{\partial v}{\partial y}^2 + \frac{\partial v}{\partial z}^2$ and $\text{div}(f) = \frac{\partial f}{\partial x} + \frac{\partial f}{\partial y} + \frac{\partial f}{\partial z}$.

The Algorithm 1 used to minimize $AT_{\varepsilon,\sigma}(f, v)$ is composed of two subroutines. The first subroutine shown in Algorithm 2, minimizing $AT_{\varepsilon,\sigma}(f, v)$ in the image variable, uses a customized version of the conjugate gradient method. The second subroutine, minimizing $AT_{\varepsilon,\sigma}(f, v)$ in the edge variable, use a projected steepest descent method.

$f^0 = 0$ or a-priori image;
$v^0 = 1$;
for $i = 0$ *to* $Iterations_{Alt} - 1$ **do**
  $\mathbf{f}^{i+1}$: $\mathbf{f}^i$ move along $-\nabla_f AT_{\varepsilon,\sigma}(\mathbf{f}, \mathbf{v}^i)$;
  $\mathbf{v}^{i+1}$: $\mathbf{v}^i$ move along $-\nabla_f AT_{\varepsilon,\sigma}(\mathbf{f}^{i+1}, \mathbf{v})$;
end

Algorithm 1: Alternate Minimization of $AT_{\varepsilon,\sigma}(\mathbf{f}, \mathbf{v})$

$\mathbf{f}^0 =$ current image;
$\mathbf{v} =$ current edge ;
$\mathbf{d}^0 = \mathcal{R}^*(\mathcal{K}_\sigma(\mathbf{g}) - \mathcal{R}_\Phi(\mathbf{f}^0)) + \alpha\text{div}(\mathbf{v}^2\nabla\mathbf{f}^0)$;
$\mathbf{p}^1 = \mathbf{d}^0$;
for $i = 1$ *to* $Iterations_{image} - 1$ **do**
  $c_1^i = \langle \mathbf{p}^i, \mathbf{d}^{i-1} \rangle_{L^2} / (\|\mathcal{R}_\Phi(\mathbf{p}^i)|^2_{L^2} + \|\mathbf{v}^2\nabla\mathbf{p}^i\|^2_{L^2})$;
  $\mathbf{f}^i = \mathbf{f}^{i-1} + c_1^i \mathbf{d}^i$;
  $\mathbf{d}^i = \mathcal{R}^*_\Phi(\mathbf{g} - \mathcal{R}_\Phi(\mathbf{f}^i)) + \alpha\text{div}(\mathbf{v}^2\nabla\mathbf{f}^i)$;
  $c_2^i = -\langle \mathcal{R}_\Phi(\mathbf{d}^i), \mathcal{R}(\mathbf{p}^i) \rangle_{L^2} / \|\mathcal{R}_\Phi(\mathbf{p}^i)|^2_{L^2}$;
  $\mathbf{p}^{i+1} = \mathbf{d}^i + c_2^i \mathbf{p}^i$;
end

Algorithm 2: Image Minimization with Conjugated Gradients

IV. Applications

A. Reconstructions with alternating minimization algorithm and artifact reduction strategy

We reconstruct the 3D Shepp-Logan phantom using the alternating minimization scheme described in Algorithm 1 and artifact reduction strategy in Sec. II-C. Slices of the original phantom, reconstructed images and segmentations are shown in Fig.1. The tilt angular range is $-60^\circ \sim 60^\circ$. Fig.1(a) is a slice of original Shepp-Logan phantom. (b)(c) show the reconstruction and segmentation without the artifact reduction strategy and (d)(e) with cutoff function $\mathcal{K}_\sigma$ defined

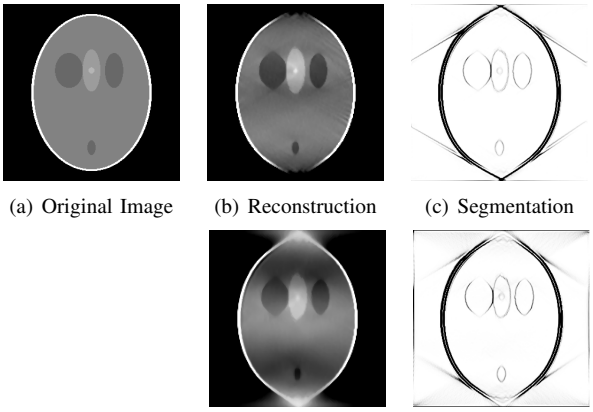

(a) Original Image (b) Reconstruction (c) Segmentation

(d) Reconstruction with strategy (e) Segmentation with strategy

Fig. 1. Reconstructions and segmentations with artifact reduction strategy

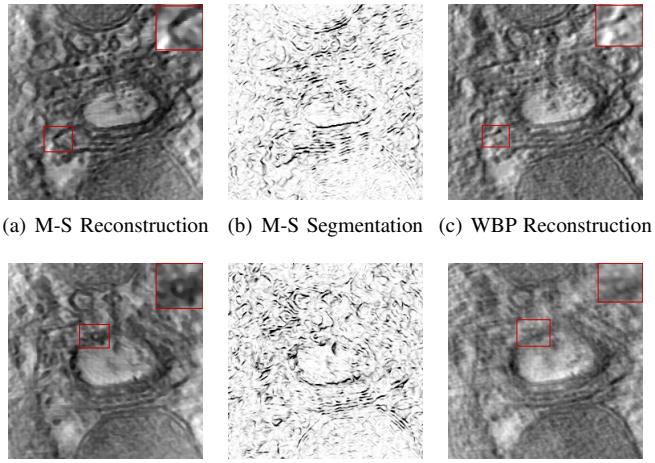

(a) M-S Reconstruction (b) M-S Segmentation (c) WBP Reconstruction

(d) M-S Reconstruction (e) M-S Segmentation (f) WBP Reconstruction

Fig. 2. Reconstructions and segmentations of cryo-specimen

in eq. (6). The effect of artifacts can be observed near $\pm 60^\circ$ in (b)(c) whereas some streak artifacts are smoothed in (d)(e). Because the projections are weighted differently by $\mathcal{K}_\sigma$ according to their directions, some uniform parts of the phantom may become uneven in the reconstructed image. Since the function $\mathcal{K}_\sigma$ is smooth, no strong edge is introduced.

B. Applications on cryo-electron tomography

We use a FEI tecani 20 TEM to detect the cryo-specimen from adult rat cardiac myocytes isolation. The tilt geometry is single-axis tilt. The experimental procedures involving animal models described in this paper were approved by the Institutional Animal Care and Use Committee of Peking University Measurements are taken along 121 equally spaced angles between $-60^\circ \sim 60^\circ$ at 1° intervals. The WBP method and the alignment of projection data are done by the TOM toolbox [13]. Two slices of the reconstructed results are shown in fig.2. We zoom in the image in the red block and put in the top right corner. Compared to the reconstructions with WBP method, the noise and artifacts in our reconstructions are reduced with our method while the edges are preserved and enhanced.

We analyzed the resolution of cryo-specimen reconstruction with the method in [14]. The voxel size of input map is 4.60 Å. The mean resolution of WBP is 17.17Å while the mean resolution of our reconstruction with alternative minimization algorithm is 15.07Å.

V. Conclusion

In this article, we have combined the artifact reduction strategy and the reconstruction method with the Mumford-Shah functional. The applications show that, for the ET data, this reconstruction method can reduce the noise and artifacts caused by the limited data problem while preserving and enhancing the edges in the reconstructed image.

VI. Acknowledgments

This work was partially supported by the National Basic Research Program of China (973 Program) (2015CB351803), the National Science Foundation of China (61421062, 61520106004), and Sino-German Center (GZ 1025), Microsoft Research of Asia.

References

[1] Ludwig Reimer. *Transmission electron microscopy : physics of image formation and microanalysis*. Springer-Verlag, 1989.

[2] Gabor T. Herman and Joachim Frank. *Computational Methods for Three-Dimensional Microscopy Reconstruction*. Springer New York, 2014.

[3] Esther Klann. A mumford-shah-like method for limited data tomography with an application to electron tomography. *Siam Journal on Imaging Sciences*, 4(4):1029–1048, 2011.

[4] Michael Radermacher. *Electron Tomography: Methods for Three-Dimensional Visualization of Structures in the Cell*, chapter Weighted Back-projection Methods, pages 245–273. Springer New York, New York, NY, 2006.

[5] S. Lanzavecchia, F. Cantele, P. L. Bellon, L. Zampighi, M. Kreman, E. Wright, and G. A. Zampighi. Conical tomography of freeze-fracture replicas: a method for the study of integral membrane proteins inserted in phospholipid bilayers. *Journal of Structural Biology*, 149(1):87–98, 2005.

[6] G. A. Zampighi, L. Zampighi, N. Fain, E. M. Wright, F. Cantele, and S. Lanzavecchia. Conical tomography ii: A method for the study of cellular organelles in thin sections. *Journal of Structural Biology*, 151(3):263–74, 2005.

[7] Guido A. Zampighi, Cataldo Schietroma, Lorenzo M. Zampighi, Michael Woodruff, Ernest M. Wright, and Nicholas C. Brecha. Conical tomography of a ribbon synapse: Structural evidence for vesicle fusion. *Plos One*, 6(3):e16944, 2011.

[8] Eric Todd Quinto, Ulf Skoglund, and Ozan Öktem. Electron lambda-tomography. *Proceedings of the National Academy of Sciences of the United States of America*, 106(51):21842–7, 2009.

[9] Ming Jiang, Peter Maass, and Thomas Page. Regularizing properties of the mumford shah functional for imaging applications. *Inverse Problems*, 30(3):1941–1946, 2014.

[10] Jürgen Frikel and Eric Todd Quinto. Characterization and reduction of artifacts in limited angle tomography. *Inverse Problems*, 29(12):2091–2128, 2013.

[11] David Mumford and Jayant Shah. Optimal approximations by piecewise smooth functions and associated variational problems. *Communications on Pure & Applied Mathematics*, 42(5):577–685, 1989.

[12] L. Ambrosio and V. M. Tortorelli. On the approximation of free discontinuity problems. *Boll. Un. Mat. Ital. B (7)*, 6(1):105–123, 1992.

[13] Stephan Nickell, Friedrich Förster, Alexandros Linaroudis, William Del Net, Florian Beck, Reiner Hegerl, Wolfgang Baumeister, and Jürgen M Plitzko. Tom software toolbox: acquisition and analysis for electron tomography. *Journal of Structural Biology*, 149(149):227–34, 2005.

[14] A Kucukelbir, F. J. Sigworth, and H. D. Tagare. Quantifying the local resolution of cryo-em density maps. *Nature Methods*, 11(1):63–65, 2014.